MoM Analysis of an Axisymmetric Chiral Radome

Halid Mustacoglu [1], Joseph R. Mautz [2], and Ercument Arvas [2]

[1] Anaren Microwave, Inc.
6635 Kirkville Road, East Syracuse, NY 13057, USA
hmustacoglu@anaren.com

[2] Department of Electrical Engineering and Computer Science
Syracuse University, Syracuse, NY 13244, USA
jrmautz@syr.edu and earvas@syr.edu

Abstract **─** An axisymmetric chiral radome has been analyzed numerically by using the method of moments. The chiral body is illuminated by a plane wave and the surface equivalence principle is used to replace the body by equivalent electric and magnetic surface currents. The effect of adding chirality to a dielectric radome of revolution is investigated throughout numerical results obtained for bodies of different shapes and material parameters. Chiral materials can be used to design anti-reflective structures to control scattering cross section patterns of bodies. A computer program is developed for the chiral radome of revolution and examples of numerical calculations are given for a chiral spherical radome, a chiral cylindrical radome, and a chiral Von Karman radome. Numerical results for the chiral spherical radome are in excellent agreement with the exact ones obtained by the eigenfunction solution. Moreover, the numerical results of the chiral Von Karman radome are in excellent agreement with the published results.

Index Terms - Axisymmetric radome, chiral radome, method of moments, and surface equivalence theorem.

I. INTRODUCTION

An axisymmetric chiral radome has been analyzed numerically by using Method of Moments (MoM) with the surface equivalence principle. Scattering and radiation from radomes and antenna systems with radomes have been studied in the last couple decades by using different methods, such as the ray tracing technique [1-3], the plane wave spectrum-surface integral technique [4], the MoM [5-8], the physical optics (PO) method and dielectric physical optics (DPO) technique [9], the finite element method (FEM) [10], the method of regularization (MoR) [11], the hybrid PO-MoM technique [12], the transmission-line modeling method [13], the adaptive integral method [14], the dyadic Green's function (DGF) technique [15-16], the fast Fourier transform (FFT) [17] and precorrected fast Fourier transform methods (P-FFT) [18], body of revolution (BOR) formulations of MoM [19-26], and the finite difference time domain (FDTD) method [27].

Arbitrary dielectric bodies, 3-D arbitrary lossy dielectric bodies, arbitrary conducting bodies, dielectric bodies of revolution, conducting bodies of revolution with and without apertures, dielectric radomes of revolution, chiral and/or metal coated dielectric bodies, a 2-D chiral radome of arbitrary shape, and dielectric radomes with antenna systems were investigated in [1–35] by using the methods mentioned above.

We have not found any work that uses MoM to analyze an axisymmetric 3-D chiral radome and calculates the internal fields and scattering from it. Here, we consider different shapes of axisymmetric chiral radomes to find out the effects of sizes and shapes on the internal fields and scattered fields outside by using MoM with BOR formulations. This work is a continuation of our previous work [36].

Submitted On: March 18, 2012
Accepted On: Dec. 16, 2012

II. ANALYSIS

A plane wave is incident on the homogeneous chiral shell of permittivity ε_2, permeability μ_2, and chirality ξ_2, shown in Fig. 1, where the η's are intrinsic impedances. A homogeneous region characterized by the medium parameters $\varepsilon_1 = \varepsilon_0$ and $\mu_1 = \mu_0$ surrounds the shell. $(\mathbf{E}^i, \mathbf{H}^i)$ represents the incident field produced by external sources in the absence of the shell. S_1 and S_2 represent the outer and inner surfaces of the shell, respectively. The field $(\mathbf{E}, \mathbf{H})$ in the region bounded by S_2 and the scattered field external to S_1 are of interest in this paper.

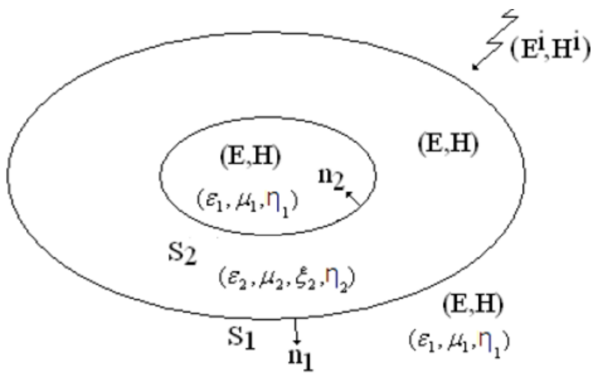

Fig. 1. A chiral radome illuminated by a plane wave.

A. Surface equivalence of the problem

Using the equivalence principle, the problem of Fig. 1 can be reduced to three simpler and equivalent problems shown in Figs. 2, 3, and 4. In the external equivalence, electric surface current $\mathbf{J}_1$ and magnetic surface current $\mathbf{M}_1$ have been placed on S_1. These surface currents are radiating in an unbounded medium of (ε_1, μ_1) with the same incident field of Fig. 1. The total field at any point in the external region bounded by S_1 in Fig. 2 is the same as the total field at the same point of Fig. 1, while the total field at any point in the internal region bounded by S_1 in Fig. 2 is zero.

$$\mathbf{E}_{1\tan}(\mathbf{J}_1, \mathbf{M}_1) = -\mathbf{E}^i_{\tan} \text{ on } S_1^- \tag{1}$$

$$\mathbf{H}_{1\tan}(\mathbf{J}_1, \mathbf{M}_1) = -\mathbf{H}^i_{\tan} \text{ on } S_1^-, \tag{2}$$

$$\mathbf{J}_1 = \mathbf{n}_1 \times \mathbf{H}^+_{out}, \tag{3}$$

$$\mathbf{M}_1 = \mathbf{E}^+_{out} \times \mathbf{n}_1, \tag{4}$$

where the superscript "–" on S_1 indicates the side of S_1 opposite the region into which $\mathbf{n}_1$ points. $\mathbf{E}_1(\mathbf{J}_1, \mathbf{M}_1)$ and $\mathbf{H}_1(\mathbf{J}_1, \mathbf{M}_1)$, respectively, denote the electric and magnetic fields produced by the surface currents $\mathbf{J}_1$ and $\mathbf{M}_1$ when they radiate in the unbounded medium of (ε_1, μ_1). $\mathbf{n}_1$ denotes the unit outward vector on S_1 and $(\mathbf{E}^+_{out}, \mathbf{H}^+_{out})$ are the total fields just outside S_1 in Fig. 1.

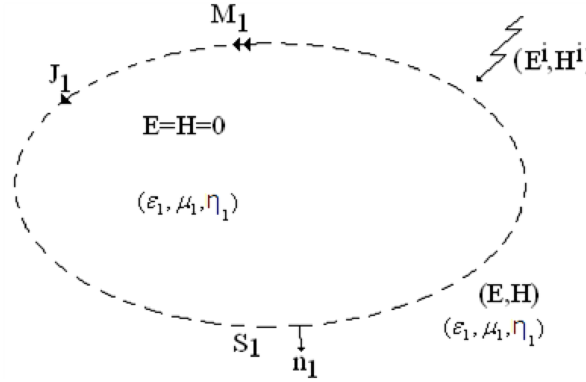

Fig. 2. External equivalence of the problem shown in Fig. 1.

In the internal equivalence for the region bounded by S_1 and S_2, surface currents $-\mathbf{J}_1$, $-\mathbf{J}_2$, $-\mathbf{M}_1$, and $-\mathbf{M}_2$ are placed on S_1 and S_2 where they radiate in the unbounded medium of $(\varepsilon_2, \mu_2, \xi_2)$. They produce the correct total fields $(\mathbf{E}, \mathbf{H})$ at any point in the region bounded by S_1 and S_2 and produce zero fields at any point outside the region bounded by S_1 and S_2.

$$\mathbf{E}_{2\tan}(\mathbf{J}_1, \mathbf{M}_1, \mathbf{J}_2, \mathbf{M}_2) = 0 \text{ on } S_1^+ \tag{5}$$

$$\mathbf{E}_{2\tan}(\mathbf{J}_1, \mathbf{M}_1, \mathbf{J}_2, \mathbf{M}_2) = 0 \text{ on } S_2^+, \tag{6}$$

$$\mathbf{H}_{2\tan}(\mathbf{J}_1, \mathbf{M}_1, \mathbf{J}_2, \mathbf{M}_2) = 0 \text{ on } S_1^+, \tag{7}$$

$$\mathbf{H}_{2\tan}(\mathbf{J}_1, \mathbf{M}_1, \mathbf{J}_2, \mathbf{M}_2) = 0 \text{ on } S_2^+, \tag{8}$$

$$\mathbf{J}_2 = \mathbf{n}_2 \times \mathbf{H}^-_{in}, \tag{9}$$

$$\mathbf{M}_2 = \mathbf{E}^-_{in} \times \mathbf{n}_2, \tag{10}$$

where S_1^+ and S_2^+ denote the sides of the surfaces S_1 and S_2 facing the regions into which the unit vectors $\mathbf{n}_1$ and $\mathbf{n}_2$ point, and $\mathbf{E}_2(\mathbf{J}_1, \mathbf{M}_1, \mathbf{J}_2, \mathbf{M}_2)$ and $\mathbf{H}_2(\mathbf{J}_1, \mathbf{M}_1, \mathbf{J}_2, \mathbf{M}_2)$, respectively, denote the electric and magnetic fields produced by the equivalent surface currents when they radiate in the unbounded medium of $(\varepsilon_2, \mu_2, \xi_2)$. $\mathbf{n}_1$ and $\mathbf{n}_2$ denote the unit vectors on S_1 and S_2, respectively and $(\mathbf{E}^-_{in}, \mathbf{H}^-_{in})$ are the total fields on S_2^- as shown in Fig. 1.

In the internal equivalence for the region bounded by S_2, surface currents $\mathbf{J}_2$, and $\mathbf{M}_2$ are placed on S_2 where they radiate in the unbounded medium of (ε_1, μ_1). They produce the correct total fields $(\mathbf{E}, \mathbf{H})$ at any point in the region bounded by

S_2 and produce zero fields at any point outside the region bounded by S_2,

$$\mathbf{E}_{1\tan}(\mathbf{J}_2, \mathbf{M}_2) = 0 \text{ on } S_2^- \quad (11)$$

$$\mathbf{H}_{1\tan}(\mathbf{J}_2, \mathbf{M}_2) = 0 \text{ on } S_2^-. \quad (12)$$

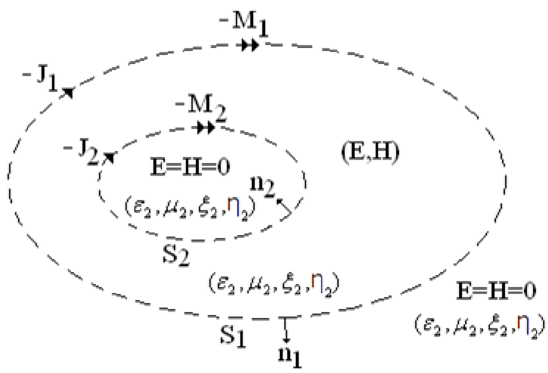

Fig. 3. Internal equivalence for the region bounded by S_1 and S_2 of the problem shown in Fig. 1.

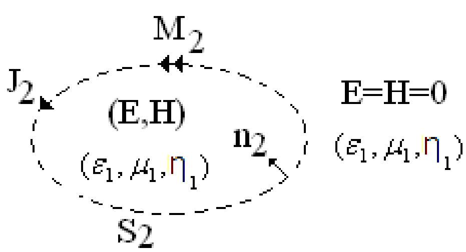

Fig. 4. Internal equivalence for the region bounded by S_2 of the problem shown in Fig. 1.

B. Formulation of the integral equations

Equations (1), (2), (5) - (8), (11), and (12) represent eight coupled integral equations for the four unknown surface currents $\mathbf{J}_1$, $\mathbf{J}_2$, $\mathbf{M}_1$, and $\mathbf{M}_2$. The combined field formulation reduces these eight equations to four by adding equations (1) to (5), (6) to (11), (2) to (7), and (8) to (12). These four coupled integral equations are solved numerically by using the method of moments.

$$-\mathbf{E}_{1\tan}(\mathbf{J}_1, \mathbf{M}_1)\Big|^{S_1^-} - \mathbf{E}_{2\tan}(\mathbf{J}_1, \mathbf{M}_1, \mathbf{J}_2, \mathbf{M}_2)\Big|^{S_1^+} = \mathbf{E}^i_{\tan} \quad (13)$$

$$-\mathbf{E}_{1\tan}(\mathbf{J}_2, \mathbf{M}_2)\Big|^{S_2^-} - \mathbf{E}_{2\tan}(\mathbf{J}_1, \mathbf{M}_1, \mathbf{J}_2, \mathbf{M}_2)\Big|^{S_2^+} = 0, \quad (14)$$

$$-\mathbf{H}_{1\tan}(\mathbf{J}_1, \mathbf{M}_1)\Big|^{S_1^-} - \mathbf{H}_{2\tan}(\mathbf{J}_1, \mathbf{M}_1, \mathbf{J}_2, \mathbf{M}_2)\Big|^{S_1^+} = \mathbf{H}^i_{\tan}, \quad (15)$$

$$-\mathbf{H}_{1\tan}(\mathbf{J}_2, \mathbf{M}_2)\Big|^{S_2^-} - \mathbf{H}_{2\tan}(\mathbf{J}_1, \mathbf{M}_1, \mathbf{J}_2, \mathbf{M}_2)\Big|^{S_2^+} = 0. \quad (16)$$

The electric and magnetic fields produced by $\mathbf{J}$ and $\mathbf{M}$ in an unbounded chiral medium are given by [37, (1.2.4) and (1.2.5)].

C. Expansion functions and testing

Let the electric and magnetic surface currents $\mathbf{J}_1$, $\mathbf{J}_2$, $\mathbf{M}_1$, and $\mathbf{M}_2$ be expanded as,

$$\mathbf{J}_1 = \sum_{n=-\infty}^{\infty} \sum_{j=1}^{N_1} \left(I^t_{1nj} \mathbf{J}^t_{1nj} + I^\phi_{1nj} \mathbf{J}^\phi_{1nj} \right) \quad (17)$$

$$\mathbf{J}_2 = \sum_{n=-\infty}^{\infty} \sum_{j=1}^{N_2} \left(I^t_{2nj} \mathbf{J}^t_{2nj} + I^\phi_{2nj} \mathbf{J}^\phi_{2nj} \right), \quad (18)$$

$$\mathbf{M}_1 = \eta_1 \sum_{n=-\infty}^{\infty} \sum_{j=1}^{N_1} \left(V^t_{1nj} \mathbf{J}^t_{1nj} + V^\phi_{1nj} \mathbf{J}^\phi_{1nj} \right), \quad (19)$$

$$\mathbf{M}_2 = \eta_1 \sum_{n=-\infty}^{\infty} \sum_{j=1}^{N_2} \left(V^t_{2nj} \mathbf{J}^t_{2nj} + V^\phi_{2nj} \mathbf{J}^\phi_{2nj} \right). \quad (20)$$

I^t_{1nj}, I^ϕ_{1nj}, I^t_{2nj}, I^ϕ_{2nj}, V^t_{1nj}, V^ϕ_{1nj}, V^t_{2nj}, and V^ϕ_{2nj} are coefficients to be determined. $\mathbf{J}^t_{1nj}$, $\mathbf{J}^\phi_{1nj}$, $\mathbf{J}^t_{2nj}$, and $\mathbf{J}^\phi_{2nj}$ are given below,

$$\mathbf{J}^t_{1nj} = \mathbf{u}_t f_{1j}(t') e^{jn\phi'} \quad (21)$$

$$\mathbf{J}^\phi_{1nj} = \mathbf{u}_\phi f_{1j}(t') e^{jn\phi'}, \quad (22)$$

$$\mathbf{J}^t_{2nj} = \mathbf{u}_t f_{2j}(t') e^{jn\phi'}, \quad (23)$$

$$\mathbf{J}^\phi_{2nj} = \mathbf{u}_\phi f_{2j}(t') e^{jn\phi'}, \quad (24)$$

$$f_{1j}(t') = \frac{1}{\rho'} T(t' - \overline{t}_{1,2j+1}), \quad (25)$$

$$f_{2j}(t') = \frac{1}{\rho'} T(t' - \overline{t}_{2,2j+1}), \quad (26)$$

$$f_{1i}(t) = \frac{1}{\rho} T(t - \overline{t}_{1,2i+1}), \quad (27)$$

$$f_{2i}(t) = \frac{1}{\rho} T(t - \overline{t}_{2,2i+1}), \quad (28)$$

$$T(t - \overline{t}_{(1,2)2i+1}) = \sum_{p=1}^{4} T_{(1,2)p+4i-4}\ \delta\ (t - t_{(1,2)p+2i-2}), \quad (29)$$

where $\delta(t)$ is the unit impulse function. The right-hand side of equation (29) is the four impulse approximation to a triangle function shown in Fig. 5. Also, t is the arc length along the generating curve of either S_1 or S_2, ϕ is the angle of the line from the origin to a specified point in the xy-plane with respect to the x-axis, ρ is the distance from the z-axis, and u_t and u_ϕ are the unit vectors in the t- and ϕ- directions, respectively. And dropping the subscripts 1 and 2 in equations (21) - (29),

$$T_{4i-3} = \frac{d^2_{2i-1}}{2(d_{2i-1} + d_{2i})} \quad (30)$$

$$T_{4i-2}=\frac{(d_{2i-1}+\frac{1}{2}d_{2i})d_{2i}}{d_{2i-1}+d_{2i}}, \tag{31}$$

$$T_{4i-1}=\frac{(d_{2i+2}+\frac{1}{2}d_{2i+1})d_{2i+1}}{d_{2i+1}+d_{2i+2}}, \tag{32}$$

$$T_{4i}=\frac{d_{2i+2}^{2}}{2(d_{2i+1}+d_{2i+2})}. \tag{33}$$

An odd number greater than or equal to 5 of consecutive points $\bar{t}_i$ at $(\bar{\rho}_i,\bar{z}_i),\ i=1,\ 2,\ ...,P$ on the generating curves of the surfaces of revolution are defined. The generating curves are approximated by drawing straight lines between the points $(\bar{\rho}_i,\bar{z}_i),\ i=1,\ 2,\ ...,P$ and we define

$$d_i=\sqrt{\left(\bar{\rho}_{i+1}-\bar{\rho}_i\right)^2+\left(\bar{z}_{i+1}-\bar{z}_i\right)^2}. \tag{34}$$

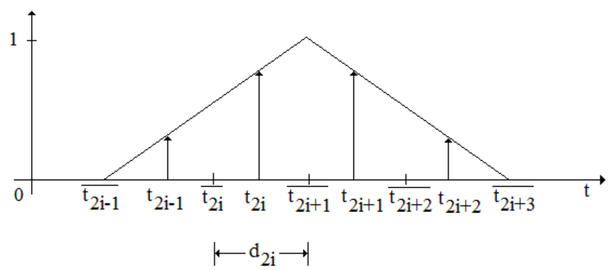

Fig. 5. Triangle function $T(t-\bar{t}_{2i+1})$ and four impulse approximation.

The quantities in equations (30) - (34) need to be specified to either the generating curve of S_1 or the generating curve of S_2. If both **h** and **g** are vector functions on S_1 or if both **h** and **g** are vector functions on S_2, then the symmetric product of **g** with **h** is $\langle \mathbf{h},\mathbf{g}\rangle$ defined as

$$\langle \mathbf{h},\mathbf{g}\rangle=\int_S \mathbf{h}\cdot\mathbf{g}\,dS, \tag{35}$$

where S is S_1 if both **g** and **h** are on S_1 and S is S_2 if both **g** and **h** are on S_2.

By taking the symmetric products of equations (13) and (15) with $\mathbf{J}_{-1ni}^{t}$ and $\mathbf{J}_{-1ni}^{\phi}$, i = 1,2,…, N_1, and taking the symmetric products of equations (14) and (16) with $\mathbf{J}_{-2ni}^{t}$ and $\mathbf{J}_{-2ni}^{\phi}$, i = 1,2,…, N_2, we obtain a matrix equation for the unknown coefficients. An incident plane wave whose propagation vector is in the *xz*-plane is considered.

D. Scattered field far from the scatterer and scattering cross section

The scattered field far from the scatterer is obtained by using the reciprocity theorem [38, Section 3-8]. For $p=\theta$ or ϕ, the p-component of the scattered field at the location $\mathbf{r}^{rec}$ of the receiver is found after some calculations to be [37, 4.6.3]

$$E_{pq}^{scat}=-\frac{j\eta_1 e^{-jk_1 r^{rec}}}{4\pi\, r^{rec}}\sum_{n=-N}^{N}\left(\tilde{R}_n^{p}T_n^{q}\right)e^{jn\phi^{rec}},\quad p,q=\theta,\ \phi, \tag{36}$$

where r^{rec} is the distance from the origin in the vicinity of the scatterer to $\mathbf{r}^{rec}$. The extra subscript q in E_{pq}^{scat} is θ for the θ-polarized incident electric field and ϕ for the ϕ-polarized incident electric field. In equation (36), the i^{th} element of T_n^q is the coefficient that multiplies the i^{th} of the $e^{jn\phi}$-dependent expansion functions for the equivalent electric and magnetic currents in the expressions for the equivalent electric and magnetic currents that radiate the far field. The contribution of the i^{th} element of $\tilde{R}_n^p$ to the far field is the right-hand side of equation (36) with the summation with respect to n replaced by the product of the three quantities which are the i^{th} element of $\tilde{R}_n^p$, the i^{th} element of $\tilde{T}_n^q$ and $e^{jn\phi^{rec}}$.

The scattering cross section σ_{pq} is the area by which the power per unit area of the incident plane wave whose electric field is q-polarized must be multiplied to obtain, by isotropic radiation, the power per unit area of the p-component E_{pq}^{scat} of the scattered electric field. Because the isotropic radiator of power P produces the power per unit area $P\big/\left(4\pi\left(r^{rec}\right)^2\right)$ at the distance r^{rec} where a receiver is located, this isotropic radiator will produce the power per unit area $\left|E_{pq}^{scat}\right|^2\big/\eta_1$ of the p-component of the scattered electric field at the distance r^{rec} if

$$\frac{P}{4\pi\left(r^{rec}\right)^2}=\frac{\left|E_{pq}^{scat}\right|^2}{\eta_1}, \tag{37}$$

where η_1 is the intrinsic impedance of the medium. Using the definition of σ_{pq} to set P equal to the product of σ_{pq} with the incident power per unit area $\left|\mathbf{E}^q\right|^2 / \eta_1$ of the q-polarized incident electric field $\mathbf{E}^q$, one obtains, after some calculations [37, 4.7.5],

$$\frac{\sigma_{pq}}{\lambda_1^{\,2}} = \frac{\left|\sum_{n=-N}^{N}\left(\tilde{R}_n^p T_n^q\right) e^{jn\phi^{rec}}\right|^2}{16\pi^3} \quad \text{where } \lambda_1 = 2\pi/k_1 . \tag{38}$$

E. Electromagnetic field inside the radome

The electromagnetic field inside the region bounded by $\mathbf{S_2}$ is calculated by using the combination of surface currents $\mathbf{J}_2$ and $\mathbf{M}_2$, radiating in all space filled with the homogeneous medium (ε_1, μ_1). The method of moment solutions for $\mathbf{J}_2$ and $\mathbf{M}_2$ are given by equations (18) and (20), respectively.

The electromagnetic field inside the region bounded by $\mathbf{S_2}$ is calculated by,

$$\mathbf{E}_i = \sum_{n=-N}^{N}\sum_{j=1}^{N_2}\Big(I_{2nj}^t \mathbf{E}_i(\mathbf{J}_{2nj}^t,\mathbf{0}) + I_{2nj}^\phi \mathbf{E}_i(\mathbf{J}_{2nj}^\phi,\mathbf{0}) + \eta_1\left(V_{2nj}^t \mathbf{E}_i(\mathbf{0},\mathbf{J}_{2nj}^t) + V_{2nj}^\phi \mathbf{E}_i(\mathbf{0},\mathbf{J}_{2nj}^\phi)\right)\Big) \tag{39}$$

$$\mathbf{H}_i = \sum_{n=-N}^{N}\sum_{j=1}^{N_2}\Big(I_{2nj}^t \mathbf{H}_i(\mathbf{J}_{2nj}^t,\mathbf{0}) + I_{2nj}^\phi \mathbf{H}_i(\mathbf{J}_{2nj}^\phi,\mathbf{0}) + \eta_1\left(V_{2nj}^t \mathbf{H}_i(\mathbf{0},\mathbf{J}_{2nj}^t) + V_{2nj}^\phi \mathbf{H}_i(\mathbf{0},\mathbf{J}_{2nj}^\phi)\right)\Big), \tag{40}$$

where the subscript i in $\mathbf{E}_\mathrm{i}$ and $\mathbf{H}_\mathrm{i}$ indicates the radiation in all space filled with the medium that is bounded by $\mathbf{S_2}$. The first argument of each of $\mathbf{E}_\mathrm{i}$ and $\mathbf{H}_\mathrm{i}$ is treated as an electric current and the second argument is treated as a magnetic current.

Using $\mathbf{E}_i(\mathbf{0},\mathbf{J}) = -\mathbf{H}_i(\mathbf{J},\mathbf{0})$ and $\mathbf{H}_i(\mathbf{0},\mathbf{J}) = \frac{1}{\eta_1^2}\mathbf{E}_i(\mathbf{J},\mathbf{0})$ to reduce all nonzero magnetic current arguments in equations (39) and (40) to zeros and then suppressing all the zero magnetic current arguments, one obtains

$$\mathbf{E}_i = \sum_{n=-N}^{N}\sum_{j=1}^{N_2}\Big(I_{2nj}^t \mathbf{E}_i(\mathbf{J}_{2nj}^t) + I_{2nj}^\phi \mathbf{E}_i(\mathbf{J}_{2nj}^\phi) - \eta_1\left(V_{2nj}^t \mathbf{H}_i(\mathbf{J}_{2nj}^t) + V_{2nj}^\phi \mathbf{H}_i(\mathbf{J}_{2nj}^\phi)\right)\Big), \tag{41}$$

$$\mathbf{H}_i = \sum_{n=-N}^{N}\sum_{j=1}^{N_2}\Big(I_{2nj}^t \mathbf{H}_i(\mathbf{J}_{2nj}^t) + I_{2nj}^\phi \mathbf{H}_i(\mathbf{J}_{2nj}^\phi) + \frac{1}{\eta_1}\left(V_{2nj}^t \mathbf{E}_i(\mathbf{J}_{2nj}^t) + V_{2nj}^\phi \mathbf{E}_i(\mathbf{J}_{2nj}^\phi)\right)\Big). \tag{42}$$

Define

$$\mathbf{Z}_{nj}^q = -\frac{1}{\eta_1}\mathbf{E}_i(\mathbf{J}_{2nj}^q), \quad q = t,\ \phi, \tag{43}$$

$$\mathbf{Y}_{nj}^q = -\mathbf{H}_i(\mathbf{J}_{2nj}^q), \quad q = t,\ \phi, \tag{44}$$

and use equations (43) and (44) in (41) and (42) to obtain

$$\mathbf{E}_i = -\sum_{n=-N}^{N}\sum_{j=1}^{N_2}\Big(\eta_1\left(I_{2nj}^t \mathbf{Z}_{nj}^t + I_{2nj}^\phi \mathbf{Z}_{nj}^\phi\right) - \eta_1\left(V_{2nj}^t \mathbf{Y}_{nj}^t + V_{2nj}^\phi \mathbf{Y}_{nj}^\phi\right)\Big), \tag{45}$$

$$\mathbf{H}_i = -\sum_{n=-N}^{N}\sum_{j=1}^{N_2}\Big(\left(I_{2nj}^t \mathbf{Y}_{nj}^t + I_{2nj}^\phi \mathbf{Y}_{nj}^\phi\right) + \left(V_{2nj}^t \mathbf{Z}_{nj}^t + V_{2nj}^\phi \mathbf{Z}_{nj}^\phi\right)\Big). \tag{46}$$

III. NUMERICAL RESULTS

The bodies analyzed in this paper, shown in Fig. 6, are illuminated by the θ-polarized plane waves. For θ^{inc} = 180º, the θ-polarized plane wave travels in the z-direction and its electric field is in the –x-direction. For θ^{inc} = 0º, the θ-polarized plane wave travels in the –z-direction and its electric field is in the x-direction.

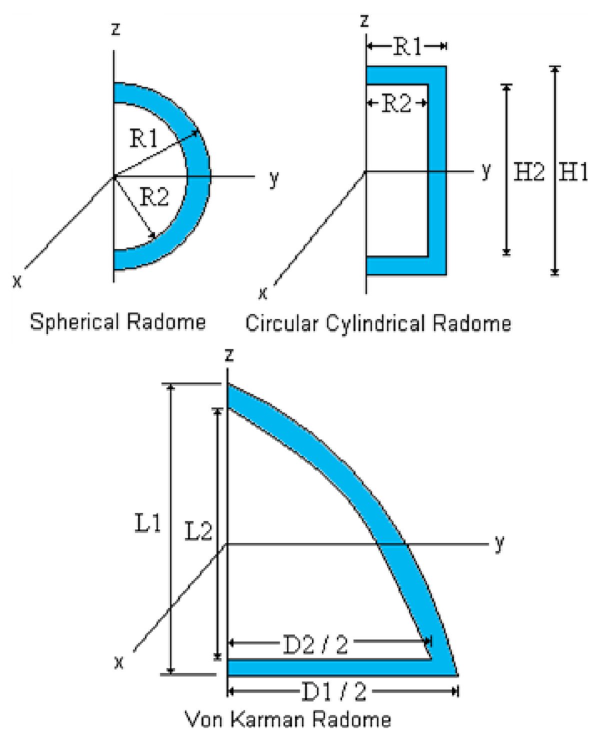

Fig. 6. Structures used to verify the method.

Numerical solution results for inside fields on the z-axis and scattering from a spherical chiral radome are presented in Figs. 7 and 8 for relative permittivity ε_r=2 and 8 and relative chirality ξ_r=0.4. The internal field plots are normalized to the incident field. The computed results are compared with the exact solution results for the spherical chiral radome and they match perfectly with each other. For ε_r=2 problem, 89 triangles on $\mathbf{S_1}$ and 79 triangles on $\mathbf{S_2}$ are used to solve for 672 unknowns, which took 6.6 minutes on a Core2Duo 2.1GHz computer. For ε_r=8 problem, 179 triangles on $\mathbf{S_1}$ and 159 triangles on $\mathbf{S_2}$ are used to solve for 1352 unknowns, which took 21 minutes on the same computer.

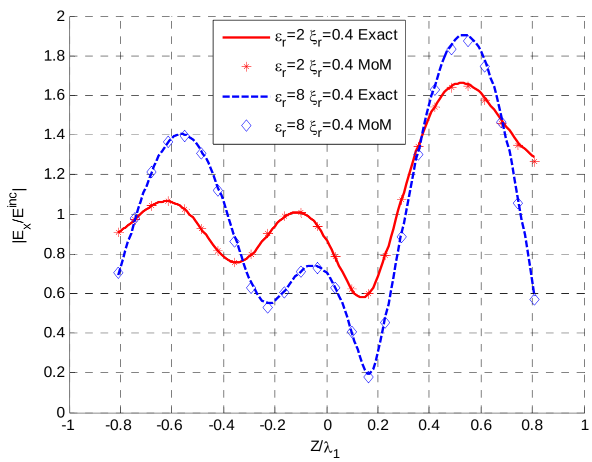

Fig. 7. Fields on the z-axis of a spherical radome for R1 = 1λ_1, R2 = 0.9λ_1, μ_r = 1, and θ^{inc} = 180º.

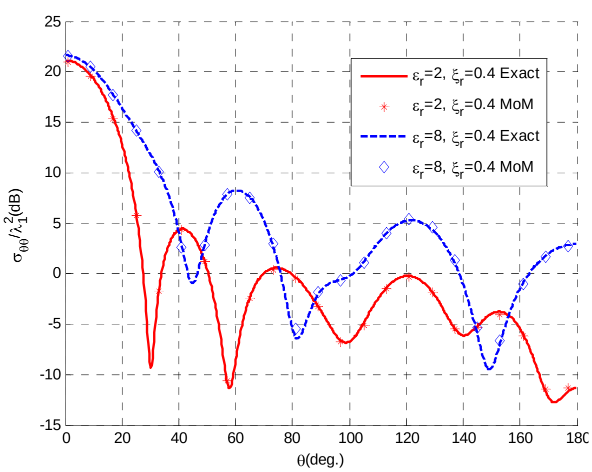

Fig. 8. $\sigma_{\theta\theta}$ of a spherical radome for R1 = 1λ_1, R2 = 0.9λ_1, μ_r = 1, and θ^{inc} = 180º.

Figures 9 and 10 show numerical results for a cylindrical radome of R1 = 1.05λ_1, R2 = 1λ_1, H1 = 10.1λ_1, H2 = 10λ_1, μ_r = 1, and θ^{inc} = 0º. For ε_r=1.55 problem, 277 triangles on $\mathbf{S_1}$ and 273 triangles on $\mathbf{S_2}$ are used to solve for 2212 unknowns. For ε_r=3 problem, 306 triangles on $\mathbf{S_1}$ and 299 triangles on $\mathbf{S_2}$ are used to solve for 2432 unknowns.

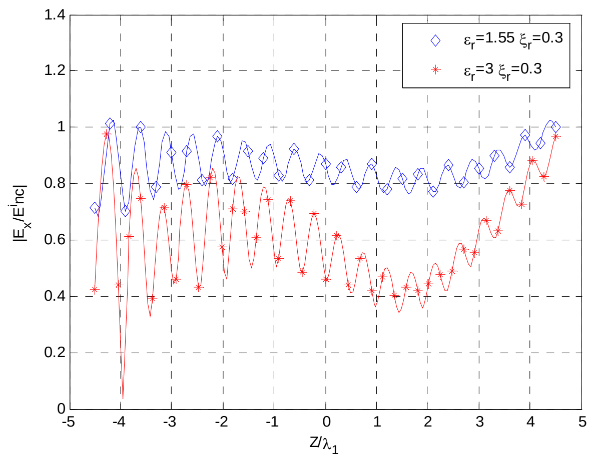

Fig. 9. Fields on the z-axis of a cylindrical radome for θ^{inc} = 0º.

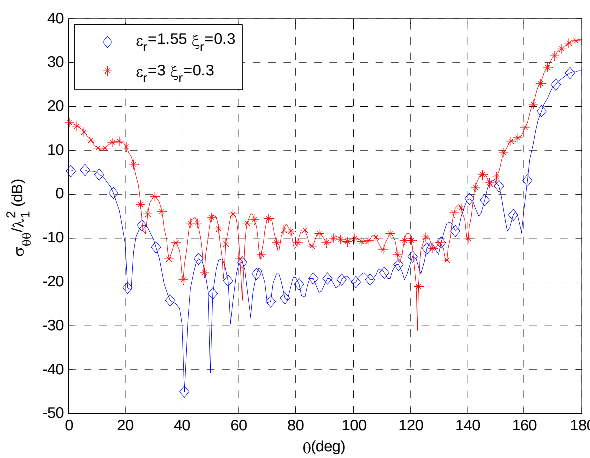

Fig. 10. $\sigma_{\theta\theta}$ of a cylindrical radome for θ^{inc} = 0º.

Results for small Von Karman radomes of different sizes and parameters were computed and validated against [33] - [35]. In Figs. 11 to 13, we show computed numerical results for a Von Karman radome of ε_r=4, L1 = 2λ_1, L2 = 1.8λ_1, D1 = 1λ_1, D2 = 0.9λ_1, ξ_r = 0, μ_r = 1 where 127 triangles are used on $\mathbf{S_1}$ and 115 triangles are used on $\mathbf{S_2}$ to solve for 980 unknowns.

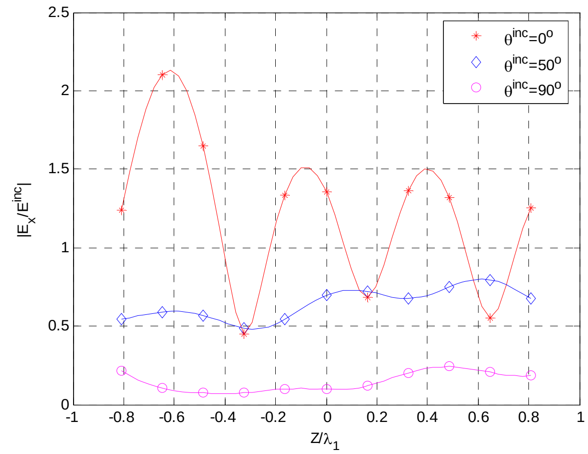

Fig. 11. Fields on the *z*-axis of a Von Karman radome for θ^{inc} = 0º, 50º, and 90º.

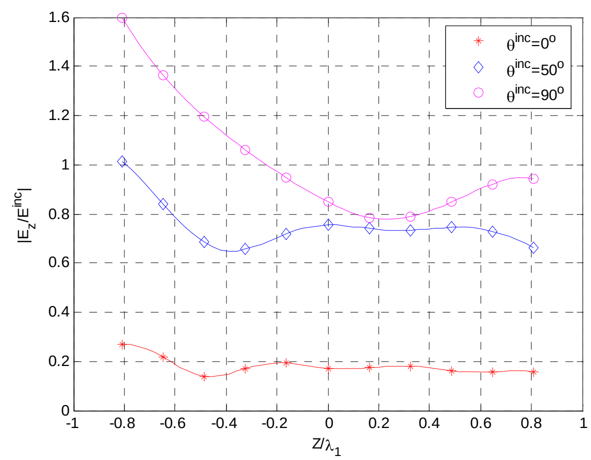

Fig. 12. Fields on the *z*-axis of a Von Karman radome for θ^{inc} = 0º, 50º, and 90º.

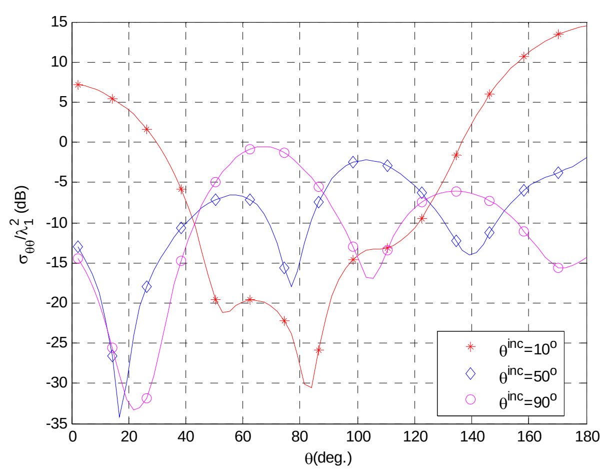

Fig. 13. $\sigma_{\theta\theta}$ of a Von Karman radome for θ^{inc} = 0º, 50º, and 90º.

More results for all these different radome structures and comparisons with previously published results are available in [37].

IV. CONCLUSION

In this paper, MoM analysis of an axisymmetric chiral radome using MoM with the surface equivalence principle is presented. The body is replaced by equivalent electric and magnetic surface currents, which produce the correct fields inside and out. The application of the boundary conditions on the tangential components of the total electric and the total magnetic fields results in a set of eight equations, which then reduces to four coupled equations that needs to be solved. Triangular expansion functions are used for both *t*-directed and ϕ-directed currents. The unknown coefficients of these expansion functions are obtained using the method of moments.

The surface currents, inside fields and the scattering cross section are computed. The results are generated by a computer code, which produces excellent agreement with the exact solution for the spherical radome and agreement with available published results for other radomes. Increasing the number of segments increases the accuracy of the solution. The radar cross section (RCS) of the radome is useful because it tells how visible the radome is from the outside. The field inside the radome due to a plane wave incident on the radome is more useful because it tells how the radome distorts radiation that comes from outside the radome. If a receiver is placed inside the radome, the field inside the radome tells how the radome affects what is received from outside. Therefore, calculations of the RCS of the radome and fields inside the radome are justified. The field radiated outside the radome by a transmitter inside the radome is also of interest. This field was not computed because of its excitation, which is the incident field of the transmitter inside the radome, is more complicated than the incident plane wave excitation used to compute the field inside the radome.

The presence of the radome affects what is transmitted and received by a transceiver placed inside the radome. Adding chirality to the radome material affects the inside fields and the scattered fields significantly for the cases studied in this paper. Although the change from no chirality to a small chirality causes cross polarized field components to evolve, thereby shifting the directions of the scattered field outside the radome and the field inside the radome away from the direction of the incident field, the effect of the chirality cannot be predicted by a simple theory. Numerical experimentation is needed.

REFERENCES

[1] J. D. Walton Jr., Ed., *Radome Engineering Handbook: Design and Principles*. New York: Marcel Dekker, 1970.

[2] D. T. Paris, "Computer-aided radome analysis," *IEEE Trans. Antennas Propagat.*, vol. 18, pp. 7-15, Jan. 1970.

[3] X. J. Gao and L. B. Felsen, "Complex ray analysis of beam transmission through two-dimensional radomes," *IEEE Trans. Antennas Propagat.*, vol. 33, pp. 963-975, Sept. 1985.

[4] D. C. F. Wu and R. C. Rudduck, "Plane wave spectrum-surface integration technique for radome analysis," *IEEE Trans. Antennas Propagat.*, vol. 22, pp. 497-500, May 1974.

[5] J. P. R. Bayard, "Analysis of infinite arrays of microstrip-fed dipoles printed on protruding dielectric substrates and covered with a dielectric radome," *IEEE Trans. Antennas Propagat.*, vol. 42, pp. 82-89, Jan. 1994.

[6] A. A. Kishk, G. Zhou, and A. W. Glisson, "Analysis of dielectric-resonator antennas with emphasis on hemispherical structures," *IEEE Antennas Propagat. Mag.*, vol. 36, pp. 20-31, April 1994.

[7] S. T. Imeci, F. Altunkilic, J. R. Mautz, and E. Arvas, "Transmission through an arbitrarily shaped aperture in a conducting plane separating air and a chiral medium," *Appl. Comp. Electromagnetics Society (ACES) Journal*, vol. 25, no. 7, pp. 587-599, July 2010.

[8] J. -Y. Li, J. -Li Guo, Y. -L. Zou, and Q. -Z. Liu, "Analysis of a cylindrical dielectric radome covering omnidirectional waveguide slot antennas," *Appl. Comp. Electromagnetics Society (ACES) Journal*, vol. 23, no. 2, pp. 166-173, June 2008.

[9] R. E. Hodges and Y. Rahmat-Samii, "Evaluation of dielectric physical optics in electromagnetic scattering," *AP-S Int. Symp. Dig.,* Ann Arbor, MI, vol. 3, pp. 1742-1745, June 1993.

[10] R. K. Gordon and R. Mittra, "Finite element analysis of axisymmetric radomes," *IEEE Trans. Antennas Propagat.*, vol. 41, pp. 975-981, July 1993.

[11] A. Y. Svezhentsev, A. I. Nosich, A. Altintas, and T. Oguzer, "Simulation of reflector antenna covered by a circular radome," *Proc. 9th Int. Conf. Antennas Propagat.,* Eindhoven, The Netherlands, pp. 532-535, April 1995.

[12] M. A. A. Moneum, Z. Shen, J. L. Volakis, and O. Graham, "Hybrid PO-MoM analysis of large axi-symmetric radomes," *IEEE Trans. Antennas Propagat.*, vol. 49, no. 12, pp. 1657-1666, Dec. 2001.

[13] R. Shavit, "Dielectric cover effect on rectangular microstrip antenna array," *IEEE Trans. Antennas Propagat.*, vol. 42, pp. 1180-1184, Aug. 1994.

[14] W. J. Zhao, L. W. Li, and Y. B. Gan, "Efficient analysis of antenna radiation in the presence of airborne dielectric radomes of arbitrary shape," *IEEE Trans. Antennas Propagat.*, vol. 53, no. 1, pp. 442-449, Jan. 2005.

[15] L. W. Li, M. S. Leong, P. S. Kooi, T. S. Yeo, and Y. L. Qiu, "Radiation of an aperture antenna covered by a spherical-shell chiral radome and fed by a circular waveguide," *IEEE Trans. Antennas Propagat.*, vol. 46, no. 5, pp. 664-671, May 1998.

[16] L. W. Li and M. S. Leong, "A 3-D discrete analysis of cylindrical radomes using dyadic Green's functions," *IEEE Antennas and Propagat. Soc. Int. Symp.*, vol. 2, pp. 846-849, 1999.

[17] Y. Zou, Q. Liu, and J. Guo, "Fast analysis of body-of-revolution radomes with method of moments," *J. of Electromag. Waves and Appl.*, vol. 21, no. 13, pp. 1803-1817, 2007.

[18] X. C. Nie, N. Yuan, L. W. Li, T. S. Yeo, and Y. B. Gan, "Fast analysis of electromagnetic transmission through arbitrarily shaped airborne radomes using precorrected-FFT method," *Progress In Electromagnetics Research, PIER,* vol. 54, pp. 37-59, 2005.

[19] S. Govind, D. R. Wilton, and A. W. Glisson, "Scattering from inhomogeneous penetrable bodies of revolution," *IEEE Trans. Antennas Propagat.*, vol. 32, no. 11, pp. 1163-1173, Nov. 1984.

[20] J. R. Mautz and R. F. Harrington, "Radiation and scattering from bodies of revolution," *Appl. Sci. Res.*, vol. 20, no. 6, pp. 405-435, June 1969.

[21] M. G. Andreasen, "Scattering from bodies of revolution," *IEEE Trans. Antennas Propagat.,* vol. 13, no. 2, pp. 303-310, March 1965.

[22] A. A. Kucharski, "A method of moments solution for electromagnetic scattering by inhomogeneous dielectric bodies of revolution," *IEEE Trans. Antennas Propagat.*, vol. 48, no. 8, pp. 1202-1210, Aug. 2000.

[23] J. R. Mautz and R. F. Harrington, "Electromagnetic scattering from a homogeneous material body of revolution," *AEŰ*, vol. 33, pp. 71-80, 1979.

[24] A. W. Glisson and D. R. Wilton, "A simple approach to the problem of coupling through azimuthally symmetric apertures in bodies of revolution," *IEEE Antennas and Propagat. Soc. Int. Symp.*, pp. 215–218, May 1978.

[25] J. R. Mautz and R. F. Harrington, "H–Field, E–Field and combined field solutions for bodies of revolution," *Technical Report TR-77-2, Department of Electrical and Computer Engineering*, Syracuse University, Syracuse, NY, pp. 13244-1240, Feb. 1977. See also J. R. Mautz and R. F. Harrington, "H–Field, E–Field and combined field solutions for conducting bodies of revolution," AEŰ, vol. 32, no. 4, pp. 157–164, Apr. 1978.

[26] J. R. Mautz and R. F. Harrington, "Electromagnetic scattering from a homogeneous body of revolution", *Technical Report TR-77-10*, Department of Electrical and Computer Engineering, Syracuse University, Syracuse, NY, 13244, Nov. 1977.

[27] B. Lin, S. Du, H. Zhang, and X. Ye, "Design and simulation of frequency-selective radome together with a monopole antenna," *Appl. Comp. Electromagnetics Society (ACES) Journal*, vol. 25, no. 7, pp. 620-625, July 2010.

[28] A. E. Fathy, "Design of a near field protective dielectric radome "window" for a curved phased array antenna-axial polarization case," *Appl. Comp. Electromagnetics Society (ACES) Journal*, vol. 23, no. 4, pp. 326-335, Dec. 2008.

[29] R. F. Wallenberg and R. F. Harrington, "Radiation from apertures in conducting cylinders of arbitrary cross section," *IEEE Trans. Antennas Propagat.*, vol. 17, no. 1, pp. 56-62, Jan. 1969.

[30] C. N. Chiu and C. I. G. Hsu, "Scattering and shielding properties of a chiral-coated fiber-reinforced plastic composite cylinder," *IEEE Trans. Electromag. Compat.*, vol. 47, no. 1, pp. 123-130, Feb. 2005.

[31] W. B. Wang and J. P. Xu, "An efficient method for analysis of EM performance of thin dielectric radomes together with wire antennas," *ICMMT2008 Proceedings*, pp. 778-780, April 2008.

[32] J. R. Mautz and R. F. Harrington, "A combined-source solution for radiation and scattering from a perfectly conducting body," *IEEE Trans. Antennas Propagat.*, vol. 27, no. 4, pp. 445-454, July 1979.

[33] E. Arvas and S. Ponnapalli, "Scattering cross section of a small radome of arbitrary shape," *IEEE Trans. Antennas Propagat.*, vol. 37, no. 5, pp. 655-658, May 1989.

[34] E. Arvas, A. Rahhalarabi, U. Pekel, and E. Gundogan, "Electromagnetic transmission through a small radome of arbitrary shape," *IEE Proceedings*, vol. 137, no. 6, pp. 401-405, Dec. 1990.

[35] E. Arvas and E. Gundogan, "Electromagnetic transmission through a small radome of arbitrary shape," *Technical Report TR-90-3*, Department of Electrical and Computer Engineering and The New York State Center for Advanced Technology in Computer Applications and Software Engineering (CASE), Syracuse University, Syracuse, NY, 13244, April 1990.

[36] H. Mustacoglu, J. R. Mautz, and E. Arvas, "Method of moments analysis of an axisymmetric chiral radome," *General Assembly and Scientific Symposium*, 2011 XXXth URSI, Oct. 2011.

[37] H. Mustacoglu, *MoM analysis of an axisymmetric chiral radome*, PhD. Dissertation, Syracuse University, Dec. 2010.

[38] R. F. Harrington, *Time-Harmonic Electromagnetic Fields.* New York: McGraw-Hill, 1961.

Halid Mustacoglu was born in Kocaeli, Turkey, in 1980. He received the B.Sc. degree in Electronics and Communication Engineering from Yildiz Technical University, Istanbul, Turkey, in 2002 and the M.Sc. and Ph.D. degrees in Electrical Engineering from Syracuse University, Syracuse, NY, in 2005 and 2011, respectively.

From 2002 to 2003, he was a Research Assistant at Syracuse University and between 2003 and 2004 he was an intern at Herley Microwave, working on microwave filter designs. From 2004 to 2011, he was a co-op at Anaren Microwave, Inc., where he worked on passive component designs. Since 2011, he has been an RF/Microwave Engineer at Anaren Microwave, Inc., where he designs RF/Microwave components. His research interests include RF/Microwave design, scattering problems, and computational electromagnetics.

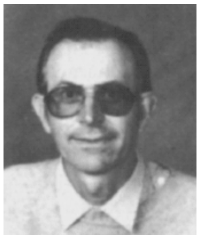

Joseph R. Mautz was born in Syracuse, NY, in 1939. He received the B.Sc., M.Sc., and Ph.D. degrees in Electrical Engineering from Syracuse University in 1961, 1965, and 1969, respectively.

Until July 1993, he was a Research Associate with the Electrical Engineering and Computer Science Department, Syracuse University, where he worked on radiation and scattering problems. Currently, he is affiliated with the Electrical Engineering and Computer Science Department at the same university. His primary fields of interest are electromagnetic theory and applied mathematics.

Ercument Arvas received the B.Sc. and M.Sc. degrees from the Middle East Technical University, Ankara, Turkey, in 1976 and 1979, respectively, and the Ph.D. degree from Syracuse University, Syracuse, NY, in 1983, all in Electrical Engineering.

From 1984 to 1987, he was with the Electrical Engineering Department, Rochester Institute of Technology, Rochester, NY. In 1987, he joined the Electrical Engineering and Computer Science Department, Syracuse University, where he is currently a Professor in the Electrical Engineering and Computer Science Department. His research and teaching interests are in electromagnetic scattering and microwave devices.